Acta Oceanol. Sin., 2024, Vol. 43, No. 11, P. 12–25
https://doi.org/10.1007/s13131-024-2433-5
http://www.aosocean.com
E-mail: ocean2@hyxb.org.cn

Carbonate system in the subtropical Jiulong River Estuary and CO_2 flux estimation under modulation of tidal cycle

Weicong Chen[1], Heng Sun[1], Zhongyong Gao[1, 2*], Jiaming Lin[2], Min Xu[2], Aijun Wang[3, 4, 5], Shuqin Tao[3, 4, 5]

[1] Key Laboratory of Global Change and Marine Atmospheric Chemistry, Third Institute of Oceanography, Ministry of Natural Resources, Xiamen 361005, China

[2] School of Marine Biology, Xiamen Ocean Vocational College, Xiamen 361100, China

[3] Laboratory of Coastal and Marine Geology, Third Institute of Oceanography, Ministry of Natural Resources, Xiamen 361005, China

[4] Fujian Provincial Key Laboratory of Marine Physical and Geological Processes, Xiamen 361005, China

[5] Observation and Research Station of Island and Costal Ecosystem in the Western Taiwan Strait, Ministry of Natural Resources, Xiamen 361005, China

Received 10 November 2023; accepted 28 February 2024

Abstract

Estuaries are often a significant source of atmospheric CO_2. However, studies of carbonate systems have predominantly focused on large estuaries, while smaller estuaries have scarcely been documented. In this study, we collected surface and bottom seawater carbonate samples in the subtropical Jiulong River Estuary across different tidal levels from 2019 to 2021. The results showed that estuarine mixing of freshwater from the river with seawater was the dominant factor influencing the estuarine carbonate system. Moreover, estuarine mixing is concomitantly impacted by the net metabolism of biological production and decomposition, groundwater input, release of CO_2 from the estuary, and precipitation or dissolution of calcium carbonate. The estuarine partial pressure of CO_2 (pCO_2) varied from 530 μatm to 7 715 μatm, which represents a strong source of atmospheric CO_2. The mean annual air-sea CO_2 flux estimated from three different parameterized equations was approximately (25.63 ± 10.25) mol/(m^2·a). Furthermore, the annual emission to the atmosphere was approximately (0.031 ± 0.012) Tg C, which accounts for a mere 0.007 7%–0.015% of global estuarine emissions. Dissolved inorganic carbon (DIC), total alkalinity (TA) and the pCO_2 exhibited high variability throughout the tidal cycle across all cruises. Specifically, the disparities observed between DIC and TA during low and high tides at identical stations during all cruises ranged from approximately 15% to 30%. The variance in the pCO_2 was even more pronounced, ranging from approximately 30% to 40%. Thus, tidal discrepancies may need to be taken into consideration to estimate the CO_2 flux from estuarine systems more accurately.

Key words: carbonate system, tidal cycle, estuarine mixing, Jiulong River Estuary

Citation: Chen Weicong, Sun Heng, Gao Zhongyong, Lin Jiaming, Xu Min, Wang Aijun, Tao Shuqin. 2024. Carbonate system in the subtropical Jiulong River Estuary and CO_2 flux estimation under modulation of tidal cycle. Acta Oceanologica Sinica, 43(11): 12–25, doi: 10.1007/s13131-024-2433-5

1 Introduction

Estuaries are among the most productive marine ecosystems and are generally considered to be semienclosed areas connected to the outer sea, where seawater is significantly diluted by freshwater from land runoff (Gattuso et al., 1998; Pritchard, 1967). Estuaries are subject to both tidal and runoff actions; they are water bodies with short retention times and circulation periods and rapidly changing hydrodynamic conditions. In addition, estuarine deltas are often human gathering places, and rivers import large amounts of organic matter and nutrients into estuaries, which are generally characterized by pronounced physicochemical gradients, active biology, and strong sedimentation dynamics (Abril and Borges, 2005). After dividing the global ocean into estuaries (0.3%), the continental shelf (7.2%), and the open ocean (92.5%), the contribution of estuaries to the carbon balance is significant despite their small size (Walsh, 1988). The CO_2 fluxes released to the atmosphere from estuaries are numerically equal to those from the continental shelf, and both play a significant role in global carbon flux (Borges et al., 2005; Cai et al., 2006; Takahashi et al., 2002, 2009). Therefore, it is necessary to study the carbonate system in estuaries to evaluate the global carbon cycle.

Historical studies have shown that estuaries are generally sources of atmospheric CO_2, with inner estuaries being strong sources and outer estuaries being weak sources or weak sinks. Chen assessed air-sea CO_2 fluxes from 165 estuaries worldwide and found that mid-latitude estuaries export the most CO_2 to the atmosphere, followed by low-latitude estuaries and high-latitude estuaries. CO_2 flux is related to water temperature, seawater residence time, and complex biogeochemical processes (Chen et al., 2013). Due to shallow and easily churned water, turbidity in in-

Foundation item: The Scientific Research Foundation of Third Institute of Oceanography, MNR under contract Nos. 2022001, 2020017, 2023008 and 2019018; the Natural Science Foundation of Fujian Province of China under contract No. 2023J01209; the National Natural Science Foundation of China under contract No. 4237061213; the Fujian Science and Technology Innovation Leader Project.
*Corresponding author, E-mail: gao@tio.org.cn

ner estuaries is usually high, biological photosynthesis is inhibited, and a high nutrient input leads to increased biological respiration. When organic carbon consumption is higher than production, the estuary is in a state of heterotrophic metabolism (Hellings et al., 2001), but this does not necessarily mean that the estuary is transporting CO_2 to the atmosphere.

Many studies have revealed that the carbonate system in estuaries is significantly influenced by tidal forcing in addition to processes such as riverine inputs, biological respiration and photosynthesis, mineralization of organic matter, and precipitation and dissolution of calcium carbonate. Dai et al. (2009) found a negative correlation between tidal height and pCO_2 in estuaries along the Taiwan Strait and suggested that tidal mixing is the main process controlling the change of pCO_2 in surface seawater. Liu et al. (2019) revealed that the sea surface pCO_2 was mainly controlled by tidal mixing except in summer on a daily scale in Hangzhou Bay.

Currently, most studies of estuarine carbonate systems and carbon fluxes have focused on large estuarine deltas, with less research having been done on smaller estuaries. There have been few studies on the carbonate system in the Jiulong River Estuary (JRE), although, in recent years, Yin et al. (2020) reported inorganic carbon dynamics in the Jiulong River basin and estuary and explored the process of additional inorganic carbon production through isotope analyses. However, Yin et al. (2020) did not consider the strong tidal action in the Jiulong River estuary. In this study, we analyze tidal variation for a more in-depth understanding of the JRE. We also report the level of air-sea CO_2 fluxes in the JRE, which has not been discussed previously.

The aim of this study was to analyze seawater samples collected throughout the salinity gradient in different seasons and at different tides and to use data on various parameters of the carbonate system, as well as temperature, salinity, dissolved oxygen, and turbidity, to investigate the mechanism of the rapid change in the estuarine carbonate system in the tidal cycle. In addition, we sought to clarify the sources and sinks of inorganic carbon and to evaluate the level of CO_2 fluxes at the air-sea interface of the JRE, thus contributing to the assessment of carbon emissions from subtropical estuaries.

2 Materials and methods

2.1 *Study site*

The JRE (Fig. 1) is located in the southeastern part of Fujian Province, China (24.37°–24.50°N, 117.75°–118.15°E) and is influenced by a monsoon climate, with obvious seasonal variation in rainfall. Annual precipitation falls within the range of 1 400–1 800 mm, precipitation is abundant from May to September and dry from October to January (Li et al., 2023). The JRE is a shallow estuary with a water depth of approximately 3–18 m (Li et al., 2011). The Jiulong River is the second largest river in Fujian Province, with a large catchment area and three major tributaries (the northern stream, western stream, and southern stream) converging in the JRE. The JRE is subject to variation in tidal influence and is dominated by semidiurnal tides, with a maximum difference of 5 m in tide level. The water is rapidly renewed, and Wang et al. (2015) used radium isotopes to calculate an estuarine water mass residence time of only 1 day to 3 days. The dual effect of

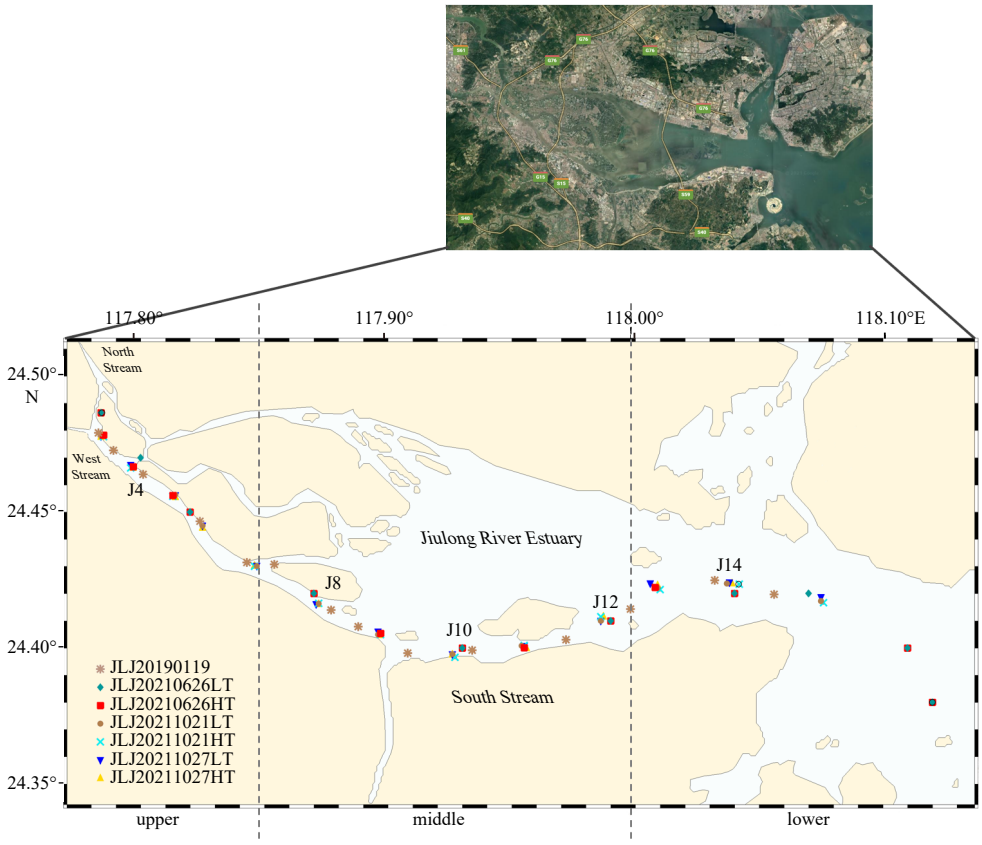

Fig. 1. Map of Jiulong River Estuary with the location of the sampling stations. Different symbols represent different cruises, and the dotted lines are the boundaries of the upper, middle, and lower reaches of the estuary. The sampling Stations J4, J8, J10, J12, J14 were consistently surveyed across the seven cruises in this study.

land runoff and tides makes for complex hydrodynamic conditions in the estuary (Li et al., 2021). There is an inhabitant population of 6.5 million people within the watershed, rapid industrialization and urbanization have caused severe anthropogenic disturbance over the past few decades. Furthermore, livestock farming is widespread in the upper reaches of the northern streams and produces large amounts of organic waste, so the JRE maintains high nutrient levels (Wu et al., 2017).

The JRE is divided into the upper estuary (117.75°–117.85°E), middle estuary (117.85°–118°E), and lower estuary (118°–118.15°E) based on differences in physical, chemical, and geomorphic environments. The upper reaches are narrow and dominated by freshwater input from the river, the middle reaches have the strongest mixing and are dominated by brackish water, and the lower reaches are close to Xiamen Bay and are dominated by saltwater input from the ocean (Yan et al., 2012).

2.2 *Surveys and sampling*

In this study, surface and bottom seawater samples were collected in different seasons from the mouths of the northern stream and western stream along a salinity gradient to the mouth of Xiamen Bay. A total of seven cruises were made: 19 January 2019 (sampling occurred during the transition from low to high tide, which is more characteristic of low tide), 26 June 2021 during low tide and high tide, and 21 and 27 October 2021 for low and high tide (Fig. 1). On 21 and 27 October 2021 (the spring tide and neap tide of that month), high tide reached 603 cm and 528 cm, respectively, according to data from Xiamen Harbor, which is close to the mouth of Xiamen Bay (www.chaoxibiao.net). The stations were set up similarly on each cruise, primarily to achieve full coverage of the salinity gradient and to facilitate observations of tidal differences.

Parameters such as temperature, salinity, DIC, total alkalinity (TA), dissolved oxygen, and turbidity were measured. DIC and TA samples were collected according to the "Guide to best practices for ocean CO_2 measurements". A 250 mL glass bottle was washed 2–3 times, the sampling tube was inserted into the bottom, and the tube was squeezed to allow seawater to spill out at a uniform rate at least half the volume of the bottle before the tube was slowly pulled out. After collecting samples, a saturated mercuric chloride solution was immediately added to the bottle to inactivate any biological activity. The bottle was then sealed by applying vacuum grease around the mouth and stopper and transported back to the land laboratory for analysis after the cruise. Temperature, salinity, dissolved oxygen, and turbidity were measured *in situ*. Temperature (±0.1℃) and salinity (±0.1) were measured with a conductivity meter (Cond 3110, WTW) and dissolved oxygen (DO) (±0.01 mg/L) was measured with a portable dissolved oxygen meter (HQ30d, HACH).

2.3 *DIC and TA measurements*

The DIC samples were analyzed with a total dissolved inorganic carbon analyzer (AS-C3, Apollo Co. USA) to quantify the total dissolved inorganic carbon in seawater based on the peak area of the infrared spectrum of the LI-7000 CO_2/H_2O analyzer with an accuracy of approximately ±2 μmol/kg. TA samples were analyzed by Gran potentiometric titration (Gran et al., 1950) using a high precision pH meter, pH electrode, and a TA titrator (AS-ALK2, Apollo Co. USA) with an accuracy of approximately ±2 μmol/kg. The methods used for DIC and TA are widely recognized (Sun et al., 2020, 2021; Wang et al., 2013).

The measurements were calibrated with Certified Reference Material (CRM) provided by Professor Dickson of the Scripps Institution of Oceanography, USA. The CRM was first analyzed to obtain 2–3 values with an error of less than 0.1% before the samples were measured. In this study, we used CRM batch #139.

2.4 *Calculations*

In this study, the carbonate system software CO2SYS was used to calculate pH and pCO_2 (Lewis and Wallace, 1998), and the value of the carbonate dissociation constant was chosen for a freshwater system (Millero, 2010). Orr et al. (2015) have pointed that the original version of Millero (2010)'s carbonate dissociation constant is subject to an error. Li et al. (2022) verified that used a value of α_5 for K_2 from Millero's unpublished spreadsheet further reduced the error. Therefore, the value of α_5 = –3.373 8 for K_2 was also used in this study to replace the α_5 = –3.374 in the original version for improved accuracy. The calculation of the sea surface pCO_2 by CO2SYS has been generally accepted as a simple and reliable method (Ries, 2011).

Temperature changes the solubility and dissociation constant of CO_2 and generally has an important influence on the sea surface pCO_2. According to the temperature effect coefficient, the sea surface pCO_2 increases by approximately 4.23% for each 1℃ increase (Takahashi et al., 1993). To eliminate the effect of temperature on the sea surface pCO_2, NpCO_2 was calculated by normalizing the temperature to the mean temperature.

$$\mathrm{N}pCO_2 = pCO_2 \cdot \mathrm{e}^{0.043(\overline{\mathrm{SST}}-\mathrm{SST})}, \tag{1}$$

where SST is the *in situ* sea surface temperature (℃), $\overline{\mathrm{SST}}$ is the mean sea surface temperature (℃) and NpCO_2 was used to remove the effect of temperature to determine the influence of other factors on the pCO_2.

The air-sea CO_2 fluxes in this study were calculated using the air-sea CO_2 partial pressure difference method, calculated as

$$\mathrm{FCO_2} = K \cdot \alpha \cdot \Delta pCO_2. \tag{2}$$

According to the new standard protocol HY/T 0343.4–2022 and HY/T 0343.7–2022 issued by the Ministry of Natural Resources of China for calculating air-sea CO_2 fluxes, and these were further amended as described below:

$$\mathrm{FCO_2} = (K \times 24 \times \alpha \times \rho \times \Delta pCO_2)/(1.013\,25 \times 10^4), \tag{3}$$

where K is the CO_2 transport rate, α is the solubility of CO_2 in seawater under certain temperature and salt conditions, and the calculation of α is now well established (Weiss, 1974). ρ is the density of surface seawater and ΔpCO_2 is the difference between the surface sea pCO_2 and atmospheric pCO_2.

$$K = k_{600} \times (Sc/600)^{-0.5}, \tag{4}$$

where Sc is the Schmidt constant for a given temperature and salt condition (Amann et al., 2015). K is generally considered to be a function dominated by wind speed, and, in this study, different wind speed parametric equations proposed by Ho et al. (2011), Van Dam et al. (2019), and Jiang et al. (2008) for shallow estuaries were used to estimate K values.

$$k_{600} = 0.06 + 0.266 \times U_{10}^2 (\text{Ho et al., 2011}), \tag{5}$$

$$k_{600} = 1.3 \times U_{10} + 3.8\ (\text{Van Dam et al., 2019}), \tag{6}$$

$$k_{600} = 3.99 - 0.436 \times U_{10} + 0.314 \times U_{10}^2 \text{ (Jiang et al., 2008)}, \quad (7)$$

where U_{10} is the wind speed at a height of 10 m. Real-time wind speeds were not measured on the ship carrying the expedition, and the wind speed data used in this study were provided by the Xiamen Gao qi International Airport monitoring station (24.48°N, 118.08°E, 14 km straight-line distance from the JRE, https://www.wunderground.com). Real-time wind speeds vary rapidly, and to better investigate tide-induced flux differences, daily average wind speeds were used for the same sampling day.

3 Results

3.1 *General water properties*

Salinity ranged from 0.15 to 32.70, generally increasing gradually from the upper to lower estuary (Table 1, Fig. 2), with low salinity near the river and high salinity near the ocean. Salinity was lowest in summer and highest in winter, but the seasonal differences were not significant. Differences in salinity due to tidal variation were pronounced, with mean salinity in the upper and middle estuary at high tide much greater than at low tide, thanks to an influx of highly saline water from the ocean to the deeper part of the estuary at high tide. Temperatures decreased slightly from the upper to lower estuary, with seasonal variation. The highest temperatures occurred in summer (as high as 30.2℃), followed by autumn, and the lowest temperatures occurred in winter (as low as 17.1℃). Overall, temperatures remained high, creating the ideal conditions for organic matter to decompose aerobically in the water column and anaerobically in the sediment.

Dissolved oxygen (DO) increased gradually from the upper to the lower estuary, approaching saturation in the lower estuary. An average dissolved oxygen value above 50% occurred for all cruises, with a maximum value of 96.8%. Although the estuary is not an anoxic environment, an overall oxygen deficit does not support the biosorption of inorganic carbon. Turbidity was greatest in the upper estuary, followed by the middle estuary, and turbidity was least in the lower estuary. This is due to the river scouring the mudflats and other environments and to the shallow depth of the estuary and the easy mixing of the water body. In surface waters, the distribution of turbidity and dissolved oxygen showed a negative correlation. High turbidity caused light limitation and inhibit biological photosynthesis, so the net effect of photosynthesis and respiration will be weakened.

Table 1. The range of temperature, salinity, dissolved oxygen concentration (DO) and turbidity parameters for all cruises, by mean±SD

Date	Tide	Temperature/℃			Salinity			DO/%			Turbidity/FTU		
		Upper	Middle	Lower	Upper	Middle	Lower	Upper	Middle	Lower	Upper	Middle	Lower
20210626	Low	28.1 ± 0.3	27.8 ± 0.3	27.9 ± 0.7	0.3	8.0 ± 7.0	28.8 ± 2.6	68.6 ± 7.3	64.6 ± 8.9	82.9 ± 2.4			
	High	28.6 ± 0.3	27.9 ± 0.5	27.3 ± 0.6	1.4 ± 1.6	21.9 ± 6.5	31.4 ± 1.8	60.5 ± 10.6	79.4 ± 8.0	93.7 ± 2.4			
20211021	Low	26.3 ± 0.2	25.7 ± 0.3	26.0 ± 0.2	1.5 ± 0.7	11.8 ± 5.6	27.7 ± 3.4	59.3 ± 6.3	53.7 ± 19.8	68.6 ± 3.3	99.4 ± 75.8	85.3 ± 36.5	61.9 ± 38
	High	25.9 ± 0.2	25.7 ± 0.2	26.1 ± 0.1	9.7 ± 6.0	25.1 ± 5.0	31.9 ± 0.5	52.9 ± 9.9	68.8 ± 12.0	79.6 ± 4.3	123.5 ± 82.8	83.7 ± 71.5	117.2 ± 113
20211027	Low	24.8 ± 0.2	24.2 ± 0.3	24.2 ± 0.2	1.6 ± 1.7	11.9 ± 5.4	27.7 ± 3.0	56.6 ± 2.8	53.7 ± 12.4	63.8 ± 8.1	77.0 ± 41.9	76.4 ± 59.7	53.2 ± 70.4
	High	25.0 ± 0.2	24.4 ± 0.1	24.4 ± 0.1	7.7 ± 4.3	23.2 ± 5.3	30.5 ± 0.7	54.4 ± 6.8	63.6 ± 10.0	70.8 ± 14.0	51.7 ± 39.3	42.4 ± 19.9	34.7 ± 21.9
20190119		19.0 ± 0.6	18.1 ± 0.5	17.5 ± 0.3	4.5 ± 3.1	14.9 ± 4.8	24.4 ± 0.9						

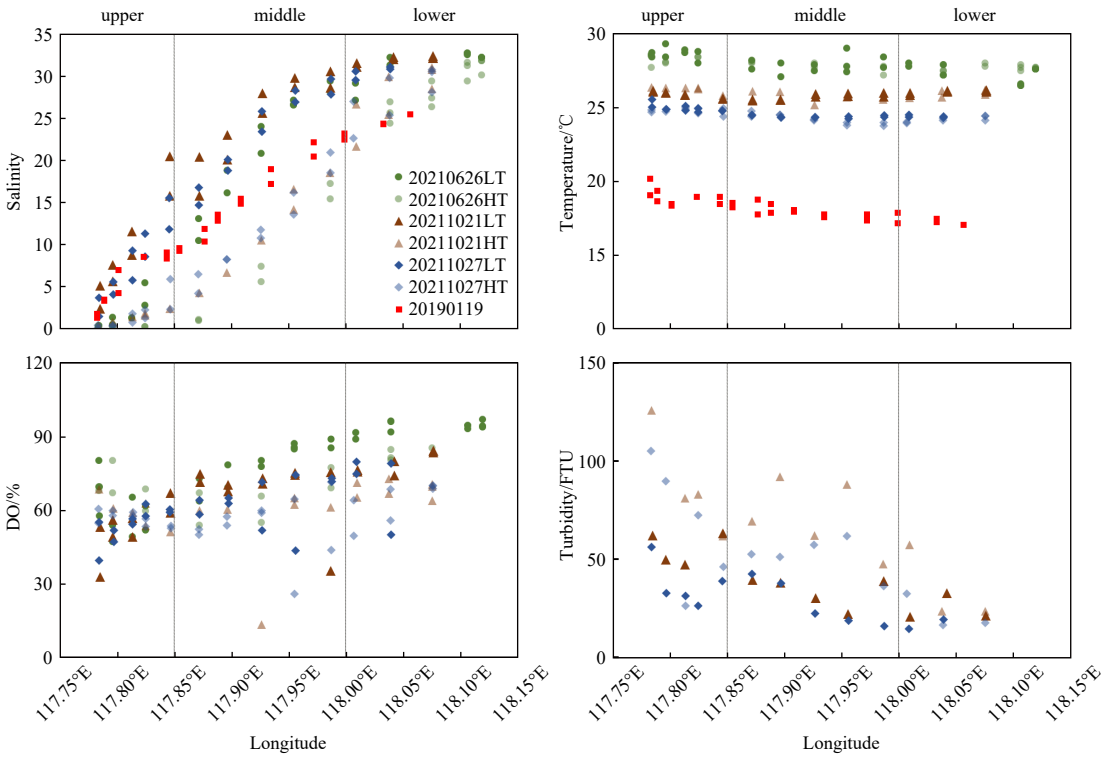

Fig. 2. The variations of salinity, temperature, DO concentration and turbidity with the longitude. HT: high tide; LT: low tide.

Without considering the state of anthropogenic factors, runoff into the JRE can be approximated as the sum of the runoff from the two hydrological stations: Punan in North Stream and Zhengdian in West Stream. Seasonal variation in runoff was plotted according to the river discharge data provided by the Ministry of Water Resources, China (http://xxfb.hydroinfo.gov.cn). The results showed that river discharge is highest in summer, followed by autumn and then winter (Fig. 3).

3.2 *Distribution of carbonate system parameters during the tidal cycle*

DIC concentrations in the JRE ranged of 956–1 971 μmol/kg, with the highest mean concentration of (1 633 ± 242) μmol/kg in winter, the second highest concentration of (1 594 ± 314) μmol/kg in autumn, and the lowest concentration of (1 549 ± 362) μmol/kg in summer (Table 2). TA varied from 790 μmol/kg to 2 145 μmol/kg, with the highest mean value of (1 633 ± 297) μmol/kg in winter, the second highest value of (1 608 ± 408) μmol/kg in autumn, and the lowest value of (1 574 ± 498) μmol/kg in summer, which was caused by dilution due to an increase in runoff after high precipitation in summer. The spatial distribution of DIC was similar to that of TA, being lowest at the riverine end, gradually increasing along the salinity gradient from the upper to lower estuary, and reaching its highest value at the oceanic end (Fig. 4) where it increased slightly with depth. pH ranged from 6.59 to 8.05, with the highest values in winter, followed by autumn, and then summer. pH also increased gradually along the salinity gradient, with low values and greater variability in the upper estuary and high, stable values in the lower estuary.

The pCO_2 in the surface waters of the JRE varied from 556 μatm to 7 761 μatm, decreasing significantly from the upper to the lower estuary, which suggests the existence of a strong CO_2 release process. The pCO_2 in the lower estuary remained higher than the atmospheric equilibrium pCO_2 (approximately 406 μatm), suggesting that the whole estuary acted as a source of atmospheric CO_2. The pCO_2 showed great seasonal variability, with mean values of (2 620 ± 2 093) μatm in summer, (1 771 ± 1 060) μatm in autumn, and (1 369 ± 880) μatm in winter. In addition, high pCO_2 values were found to be accompanied by low pH in combination with the distribution of pH.

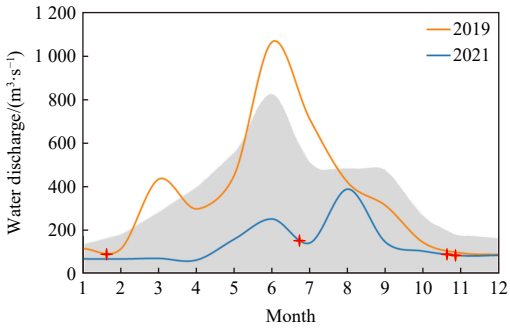

Fig. 3. The monthly average water discharge of the Jiulong River in 2019 and 2021. The shaded area shows the historical monthly average data from 1961 to 2022 and the four-pointed stars represent the dates of the survey cruises in this study.

According to tidal data from Xiamen Harbor, the difference in tidal height between high tide and low tide on the same sampling day was approximately 4–5 m, which was consistent with the water depth data obtained from sampling. High tide and low tide reflected the difference in the degree of mixing. DIC, TA, and pH in the JRE had significant tidal differences (Fig. 4): these factors were all high at high tide and low at low tide, while, in contrast, the pCO_2 is high at low tide and low at high tide. At high tide, marine salt water with high DIC, high TA, high pH, and a low pCO_2 pours deeper into the estuary, making the carbonate system throughout the estuary significantly different than it is at low tide. The 21st day, as the spring tide, compared to the 27th day, as the neap tide in October 2021, also shares the above characteristics.

The JRE is strongly influenced by tidal action, and tidal variation seriously affects the carbonate system in the estuary. The difference between DIC and TA at low tide and high tide at the same stations in all cruises ranged from approximately 15% to 30%, and the difference was approximately 30% to 40% for the pCO_2. The differences caused by tidal variation were most pronounced in the middle estuary, where the magnitude of change in DIC and TA at Station J8 was close to 40%, and the magnitude of change in the pCO_2 was close to 60%, which suggests that the changes in the estuarine carbonate system caused by the tidal cycle are more pronounced than those caused by other processes.

3.3 *CO_2 fluxes at the air-sea interface in the JRE*

Our calculations indicated that air-sea CO_2 fluxes in the JRE had significant spatial and temporal variability (Table 3). It decreased significantly from upper to lower estuary, with a mean CO_2 flux of (131.2 ± 65.07) mmol/(m²·d) in the upper, (47.7 ± 25.91) mmol/(m²·d) in the middle, and (16.64 ± 10.69) mmol/(m²·d) in the lower, which was highly similar to the spatial distribution of sea surface pCO_2. The change in ΔpCO_2 resulted in the variation of air-sea CO_2 fluxes. The ΔpCO_2 decreased signi-

Table 2. The range of carbonate parameters for all cruises, by Mean±SD. The pCO_2 data is only for the surface water, and the rest includes the surface and bottom water

Season	Cruise	Tide	DIC/(μmol·kg⁻¹)			TA/(μmol·kg⁻¹)			pH			pCO_2/μatm		
			Upper	Middle	Lower	Upper	Middle	Lower	Upper	Middle	Lower	Upper	Middle	Lower
Summer	20210626	Low	1 035 ± 45	1 281 ± 212	1 850 ± 72	867 ± 55	1 198 ± 273	1 984 ± 111	7.0 ± 0.1	7.2 ± 0.2	7.8 ± 0.1	5 599 ± 1868	3 245 ± 1 496	841 ± 187
		High	1 093 ± 76	1 664 ± 169	1 900 ± 48	952 ± 89	1 720 ± 237	2 074 ± 71	7.0	7.6 ± 0.2	7.8	4 760 ± 264	1 309 ± 613	657 ± 62
	Seasonal average			1 549 ± 362			1 574 ± 498			7.5 ± 0.4			2 620 ± 2 093	
Autumn	20211021	Low	1 115 ± 53	1 515 ± 150	1 868 ± 63	1 029 ± 72	1 503 ± 178	1 958 ± 94	7.2 ± 0.1	7.5 ± 0.1	7.7 ± 0.1	2 757 ± 649	1 527 ± 308	1 007 ± 138
		High	1 431 ± 176	1 812 ± 97	1 944 ± 11	1 397 ± 206	1 898 ± 145	2 129 ± 18	7.4 ± 0.1	7.7 ± 0.1	7.9	1 886 ± 336	922 ± 174	613 ± 12
	20211027	Low	1 072 ± 74	1 540 ± 162	1 881 ± 51	954 ± 103	1 502 ± 226	1 966 ± 79	7.1 ± 0.1	7.4 ± 0.3	7.7 ± 0.1	3 473 ± 752	1 409 ± 490	1 029 ± 192
		High	1 422 ± 207	1 811 ± 90	1 941 ± 12	1 334 ± 214	1 875 ± 136	2 092 ± 28	7.2 ± 0.1	7.7 ± 0.1	7.8	3 239 ± 622	1 013 ± 251	686 ± 65
	Seasonal average			1 594 ± 314			1 608 ± 408			7.5 ± 0.3			1 771 ± 1 060	
Winter	20190119		1 349 ± 184	1 707 ± 122	1 941 ± 23	1 306 ± 184	1 708 ± 177	2028 ± 39	7.5 ± 0.2	7.6 ± 0.2	7.8 ± 0.1	1 335 ± 656	1 576 ± 1 065	711 ± 204
	Seasonal average			1 633 ± 242			1 633 ± 297			7.6 ± 0.2			1 369 ± 880	

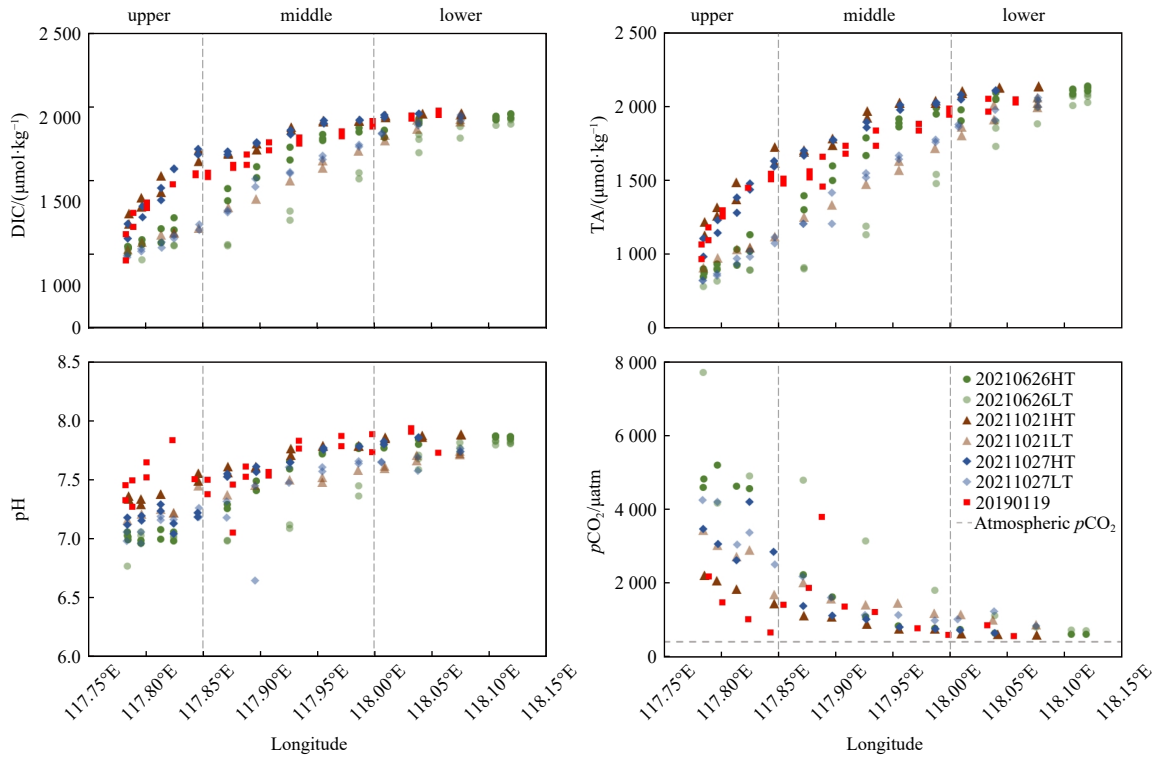

Fig. 4. Spatial distribution of carbonate system parameters during tidal cycle. HT: high tide; LT: low tide.

Table 3. CO_2 fluxes at the air-sea interface of JRE

Cruise	Zone	T/℃	S	ΔpCO_2/ μatm	U_{10}/ (m·s^{-1})	$F_{\text{Jiang(2008)}}$/ (mmol·m^{-2}·d^{-1})	$F_{\text{Van Dam(2019)}}$/ (mmol·m^{-2}·d^{-1})	$F_{\text{Ho(2011)}}$/ (mmol·m^{-2}·d^{-1})	Flux/ (mmol·m^{-2}·d^{-1})
20210626LT	Upper	28.0	0.3	5 216	2.07	199.81 ± 71.74	292.57 ± 105.04	53.99 ± 19.38	182.12 ± 120.27
	Middle	28.0	7.3	2 857	2.07	107.22 ± 58.98	157 ± 86.37	28.97 ± 15.94	97.73 ± 64.54
	Lower	27.8	27.6	449	2.07	15.08 ± 6.59	22.08 ± 9.65	4.07 ± 1.78	13.74 ± 9.08
20210626HT	Upper	28.8	1.1	4 375	2.07	167.30 ± 10.65	244.97 ± 15.59	45.20 ± 2.88	152.49 ± 100.71
	Middle	27.6	20.4	918	2.07	32.54 ± 22.91	47.65 ± 33.54	8.79 ± 6.19	29.66 ± 19.59
	Lower	27.4	30.8	263	2.07	8.61 ± 2.20	12.61 ± 3.23	2.33 ± 0.6	7.85 ± 5.18
20211021LT	Upper	26.2	1.4	2 355	3.05	113.75 ± 31.62	158.18 ± 43.97	51.75 ± 14.38	107.89 ± 53.46
	Middle	25.7	10.8	1 129	3.05	52.40 ± 15.53	72.87 ± 21.59	23.84 ± 7.06	49.71 ± 24.63
	Lower	25.8	25.2	612	3.05	26.37 ± 6.42	36.67 ± 8.93	12 ± 2.92	25.01 ± 12.39
20211021HT	Upper	25.9	8.2	1 486	3.05	69.87 ± 17.30	97.16 ± 24.06	31.78 ± 7.87	66.27 ± 32.83
	Middle	25.7	23.8	525	3.05	22.87 ± 8.23	31.81 ± 11.44	10.41 ± 3.74	21.7 ± 10.75
	Lower	26.0	31.7	216	3.05	8.89 ± 0.52	12.36 ± 0.72	4.04 ± 0.24	8.43 ± 4.18
20211027LT	Upper	24.9	1.0	3 069	4.34	213.58 ± 53.06	251.69 ± 62.53	135.16 ± 33.58	200.14 ± 59.42
	Middle	24.3	11.1	1 008	4.34	67.47 ± 34.45	79.51 ± 40.60	42.69 ± 21.8	63.22 ± 18.77
	Lower	24.1	25.3	631	4.34	39.08 ± 12.17	46.06 ± 14.34	24.73 ± 7.7	36.63 ± 10.87
20211027HT	Upper	25.1	6.4	2 836	4.34	192.46 ± 42.18	226.81 ± 49.7	121.79 ± 26.69	180.35 ± 53.54
	Middle	24.4	22.3	615	4.34	38.88 ± 16.95	45.82 ± 19.98	24.6 ± 10.73	36.43 ± 10.82
	Lower	24.4	30.2	287	4.34	17.21 ± 4.06	20.29 ± 4.78	10.89 ± 2.57	16.16 ± 4.79
20190119	Upper	19.3	5.2	929	1.6	33.35 ± 23.84	47.88 ± 34.23	6.04 ± 4.32	29.09 ± 21.24
	Middle	18.4	14.1	1 171	1.6	40.65 ± 37.38	58.36 ± 53.67	7.37 ± 6.77	35.46 ± 25.89
	Lower	17.7	23.8	308	1.6	9.99.16 ± 6.75	14.34 ± 9.69	1.81 ± 1.22	8.71 ± 6.36

ficantly at high tide compared to low tide, due to the substantial intrusion of low pCO_2 seawater from offshore into the JRE. Thus, the air-sea CO_2 fluxes of the JRE (including the upper, middle, and lower) were markedly reduced at high tides than at low tides. The potential for the entirety of the estuary to release CO_2 to the atmosphere was thereby greatly curtailed during high tide. Air-sea CO_2 fluxes were lower in winter than in summer and autumn, but all show positive values, suggesting that the whole JRE was transporting CO_2 to the atmosphere.

To estimate the annual mean air-sea CO_2 flux of the JRE, the spring pCO_2 data of Yin et al. (2020) were used for additional calculations because spring data were not obtained in this study. Averaged over different seasons, the annual mean air-sea CO_2 flux from the JRE was estimated to be approximately (25.63 ± 10.25) mol/(m^2·a). The JRE covers an area of approximately 100 km^2 (Zheng et al., 2011) and emits carbon approximately

(0.031 ± 0.012) Tg to the atmosphere annually. Historical studies have estimated annual global estuarine CO_2 emissions (in terms of C) to be approximately 0.2 Pg/a to 0.4 Pg/a, so the JRE accounts for approximately 0.007 7% to 0.015% of global estuarine emissions. Note that given many estuaries worldwide experience semi-diurnal tidal fluctuations akin to the JRE, scaling findings to the global scale impels quantifying uncertainties introduced when failing to account for such tidal oscillations in air-sea flux assessments. Annual flux estimates could underestimate or overestimate net CO_2 emissions depending on whether flux is predominately tallied during high or low tide periods.

4 Discussion

4.1 *Carbonate system during estuarine mixing*

DIC and TA in the JRE were significantly and positively correlated with salinity, and both were near the conservative mixing line (Fig. 5), reflecting the fact that the exchange of river water and ocean water is close to conservative mixing, especially in summer.

To investigate the deviation of the sample DIC from conservative mixing, we used a two end-member mixing model to calculate the DIC concentration predicted by conservative mixing of riverine freshwater and marine hypersaline water at different salinities, referring to Samant's study (Samanta et al., 2015). The DIC_{mix} value was calculated as follows:

$$DIC_{mix} = DIC_{river} \times (1 - S_{sample}/S_{ocean}) + DIC_{ocean}(S_{sample}/S_{ocean}). \quad (8)$$

Deviation of the actual level from the conservative mix was evaluated by subtracting the DIC_{mix} value from the sample DIC value, and the excess of the sample DIC relative to the DIC_{mix} value was defined as excess DIC.

$$DIC_{excess} = DIC_{sample} - DIC_{mix}. \quad (9)$$

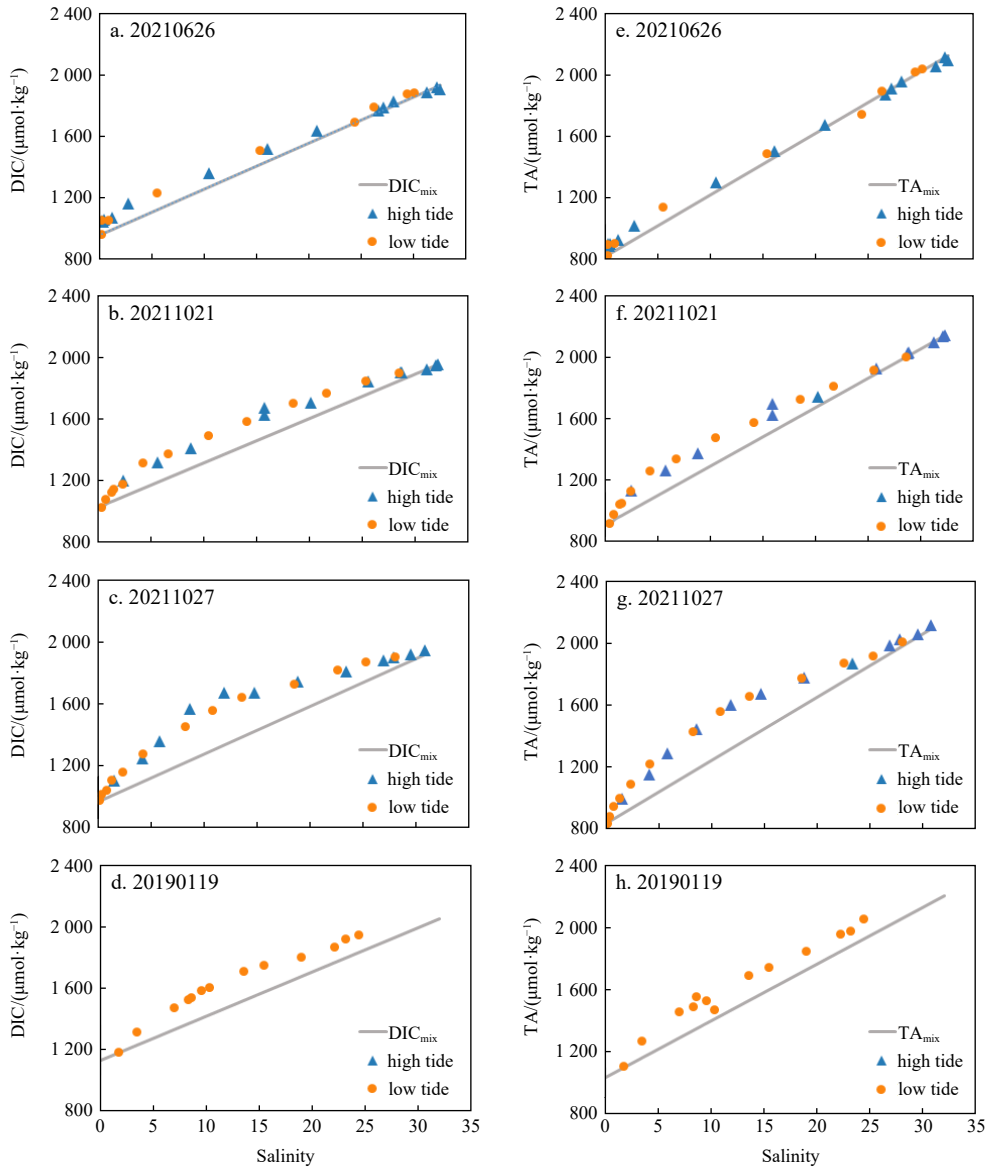

Fig. 5. Variations of DIC (a, b, c, d), TA (e, f, g, h) with salinity. Grey line is the mixing line obtained by end-member model calculation for each cruise.

Excess DIC is the sum of all DIC inputs from within the estuary. The mixing calculation for TA is similar to that for DIC and only requires that the corresponding DIC values are converted to TA values. DIC/TA is increased by respiration, decomposition of organic matter, and precipitation of calcium carbonate and decreased by photosynthesis, dissolution of calcium carbonate, and emission of CO_2. In addition, TA changes caused by the precipitation or dissolution of calcium carbonate alone are twice as large as those caused by DIC.

The DIC/TA concentrations at the stations during the summer were generally in line with the positions predicted by the conservative mixing of seawater and freshwater (Figs 5a, e). Less excess DIC/TA indicates that the variation in DIC/TA during the summer was almost entirely controlled by the conservative mixing of the river with seawater. Higher river discharge and short residence times reduce the reaction of water with the soil and sediment, allowing more carbon to flow out in a particulate state, thus making nonconservative DIC/TA inputs less pronounced. The high turbidity that prevents photosynthesis, combined with relatively low dissolved oxygen, indicates low primary production and no significant DIC removal in the estuary. Although the entry of rich DIC and TA pore water from the underground estuary of the Jiulong River into the JRE will increase DIC and TA, the output of groundwater is a nonpoint source of the estuary and will not lead to a significant increase in the mixing line under steady-state conditions (Wang et al., 2015). In addition, although the estuary is supersaturated with significant CO_2 emissions, it is likely to be compensated by CO_2 from processes such as respiration and denitrification and reach equilibrium, so no significant addition or removal of DIC occurs during mixing (Guo et al., 2008). Therefore, although a range of biogeochemical processes occur during mixing in the summer, their effects are limited relative to the mixing process.

However, in autumn and winter, several stations with significantly higher than conservative mixing concentrations (Figs 5b, c, d, f, g and h) were observed in the middle and upper estuary, suggesting that there are additional processes that produce DIC/TA. This phenomenon is slightly more pronounced at low tide than at high tide. As autumn and winter are dry seasons, low river runoff leads to less flushing, which may cause the addition of DIC/TA. CO_2 produced in sediments can increase DIC by mixing with estuarine water through tidal oscillations and pore water exchange (Jahnke et al., 2003). Additionally, under nonsteady-state conditions, groundwater output may cause DIC and TA to exhibit significant additions to the mixing line (Wang et al., 2015). Furthermore, aragonite saturation states (Ω) were calculated using CO2SYS software, and were found to be less than 1 in the upper estuary and in some parts of the middle estuary, demonstrating that the dissolution of calcium carbonate may have occurred. Overall, changes in DIC and TA in the JRE can be attributed to the combined effects of mixing processes, terrestrial runoff, aerobic respiration, remineralization of organic matter, precipitation and dissolution of $CaCO_3$, CO_2 release from the air-sea interface, and subterranean estuarine inputs.

To understand and quantify the composition of estuarine DIC, calculations were performed in conjunction with the Jiang et al. (2008) approach. It is assumed that the DIC value of the river end-member is 0, and the DIC concentration when no DIC is provided by the river and only provided by the ocean for mixing is calculated accordingly:

$$\mathrm{DIC_{mix\text{-}ocean}} = \mathrm{DIC_{ocean}}(S_{\mathrm{sample}}/S_{\mathrm{ocean}}). \tag{10}$$

As shown in Fig. 6a, the sample DIC can be numerically equal to the sum of the excess DIC, the riverine DIC, and the oceanic DIC. According to Eqs (8), (9) and (10), the riverine DIC is numerically equal to the $\mathrm{DIC_{mix}}$ minus the $\mathrm{DIC_{mix\text{-}ocean}}$, and the oceanic DIC is numerically equal to the $\mathrm{DIC_{mix\text{-}ocean}}$. The choice of end-element values is shown in Table 4.

Data from Stations J4, J8, J10, J12, and J14 were selected to analyze the composition of DIC and the differences between

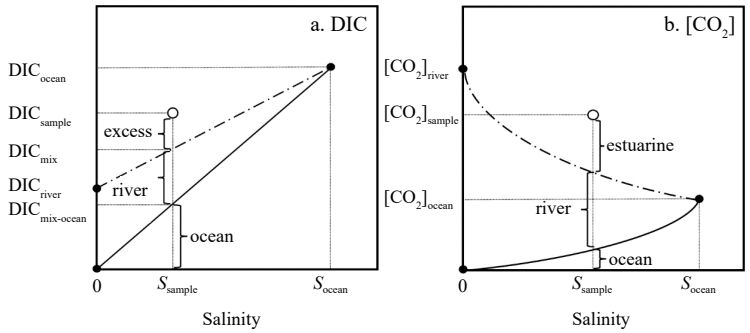

Fig. 6. Diagrams of the concentrations of DIC and dissolved CO_2 ($[CO_2]$) versus salinity during estuarine mixing. a represents the calculation of the DIC composition of the estuary, with salinity on the *X*-axis and DIC concentration on the *Y*-axis; b represents the calculation of $[CO_2]$ composition of the estuary, with salinity on the *X*-axis and dissolved CO_2 concentration on the *Y*-axis.

Table 4. End-member values of DIC and TA used in mixing model calculation

Date	River end-member			Ocean end-member		
	DIC/(μmol·kg^{-1})	TA/(μmol·kg^{-1})	Salinity	DIC/(μmol·kg^{-1})	TA/(μmol·kg^{-1})	Salinity
20210626	958	827	0.3	1 920	2 112	32.2
20211021	1 027	917	0.5	1 954	2 145	32.1
20211027	975	831	0.2	1 954	2 145	32.1
20190119	1 181	1 101	1.8	2 045	2 203	32.0

Note: The ocean end-member for January 19, 2019 utilizes Lin's observations near Xiamen Bay (Lin, 2012), and the rest is from this study. The ocean end-member for both October 21 and October 27 is identical due to the presence of low salinity at the farthest station on the latter date. Consequently, the high-salinity end-member from October 21 is selected in both cruises.

tides and seasons. The results showed that riverine and seawater mixing processes dominate, while excess DIC caused by respiration and other biogeochemical processes accounts for a small proportion (Fig. 7). Considerable spatial variability in dissolved inorganic carbon composition was observed among various regions within the estuary. Station J4 in the upper was dominated by riverine inputs. Stations J8 and J10 in the middle exhibited a signature primarily affected by riverine and seawater mixing processes. Station J14 in the lower shifted to ocean domination. Thus, the longitudinal gradient conveyed a transitioning dominion over DIC patterns—from riverine domination in the upper estuary to ocean control over composition in the Lower estuary, with mid-estuary undergoing variably balanced mixed influence from the two endmember sources under tidal dispersion and biogeochemical modification.

The proportion of excess DIC was lowest in summer and increased in autumn and winter, which is consistent with our qualitative analysis. Compared with autumn, dissolved oxygen was higher and apparent oxygen consumption was lower in summer; thus, lower excess DIC in summer may be due to enhanced photosynthesis, which reduces more excess DIC to offset some of the increased excess DIC from decomposition. The riverine DIC contribution was highest in summer, a clear signal of higher runoff, and weaker in autumn and winter, which is consistent with the historical river discharge of the Jiulong River (Fig. 3).

Excess DIC and riverine DIC were significantly more concentrated at low tide than at high tide, while oceanic DIC was the dominant component of DIC at high tide, contributing more than 70%. The differences due to tidal variation were more pronounced than differences due to seasonal variation. This difference was most accentuated evident in the middle. Particularly illustrative of this phenomenon was Station J8, where tidal fluctuations engendered a near exclusive dominance of riverine input at low tide that transformingly gave way to preponderant oceanic DIC exceeding riverine proportions during high tide. Thus, under the oscillations of the semi-diurnal tidal cycle, the JRE conveyed a drastic pendular shifts between endmember carbon sources, especially in the middle. At low tides, river flows prominent control over DIC composition; whereas, oceanic DIC surges to the fore at high tides. Overall, our quantitative calculations clearly revealed the dynamic change of DIC components throughout the estuary under tidal effect, and DIC in the estuary was dominated by the mixing of the river and seawater, which is also consistent with the findings of Yin et al. (2020).

4.2 *Factors affecting sea surface pCO_2 and dissolved CO_2 in the JRE*

Generally, seasonal variation in the pCO_2 in river-dominated estuaries is influenced by temperature and river runoff inputs (Jiang et al., 2008). The NpCO_2 values obtained by normalization of average temperature have had the effect of temperature removed, enabling us to judge the role of other influences on the sea surface pCO_2. After normalizing to an annual mean temperature of 24.9℃ to remove the effect of temperature (Fig. 8), the NpCO_2 still showed distinct seasonal characteristics and tidal differences, suggesting that temperature may not be the main cause of seasonal variation in pCO_2. The NpCO_2 is highest in summer, followed by autumn, and lowest in winter, which is consistent with seasonal variation in river discharge (Fig. 3); thus, runoff may have a strong influence on estuarine pCO_2.

Intense anthropogenic activities and high levels of nutrients in the Jiulong River Basin have led to the production of large amounts of CO_2 from respiration, organic carbon degradation, and other processes. Yin et al. (2020) found that the surface water pCO_2 of the northern stream and western stream was high (2 938–6 794 μatm), so seasonal mixing of high pCO_2 river water with low pCO_2 marine water may cause spatial and temporal variation in the pCO_2 in the estuary. Rivers with a high pCO_2 flow into the upper estuary; at the same time, due to narrow river channels and fast flow rates, these rivers can stir the bottom, make the water more turbid, and reduce the efficiency of photosynthesis, resulting in the highest pCO_2 in the upper estuary. A large amount of CO_2 has already escaped to the atmosphere by the time the ocean mixes with the river, and the pCO_2 becomes lower in the middle estuary. In the lower estuary, the pCO_2 reaches its lowest value due to the increased deposition of suspended sediments, high transparency of the water body, and nutrients carried by the river that provide conditions for photosynthesis.

Dissolved CO_2 ([CO_2]) from the river, [CO_2] from the ocean, and [CO_2] generated within the estuary together contribute to the total [CO_2] in the estuary, and the method of Jiang et al. (2008)

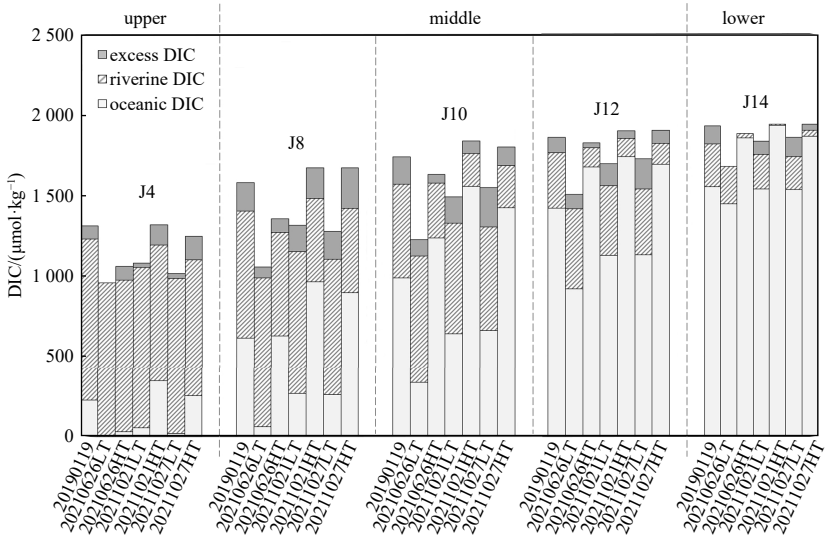

Fig. 7. Histogram of the proportion of DIC composition in the JRE. HT: high tide; LT: low tide.

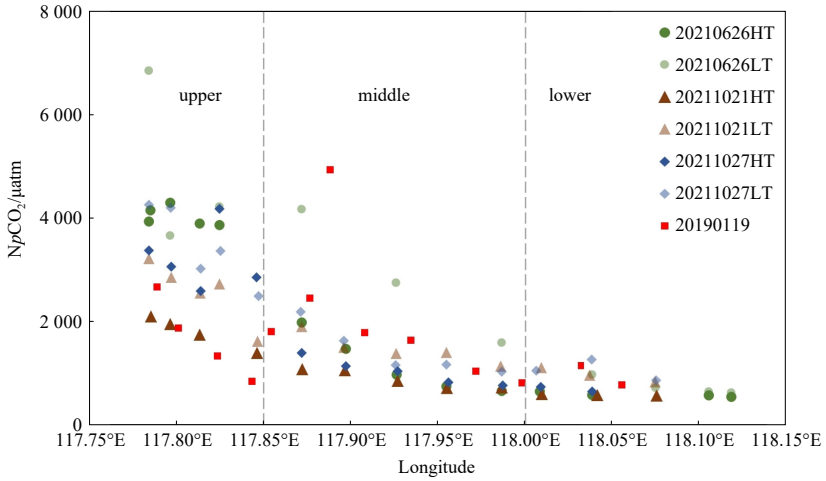

Fig. 8. Variation of NpCO_2(T = 24.9℃) with longitude in the JRE. HT: high tide; LT: low tide.

was used to quantify their respective contributions in a simple way. Similar to the calculation of DIC, estuarine [CO_2] can be calculated from the difference between the sample [CO_2] concentration and the $[CO_2]_{mix}$ from conservative mixing of seawater and freshwater, and river [CO_2] is calculated from the difference between $[CO_2]_{mix}$ and $[CO_2]_{mix\text{-}ocean}$. However, it should be noted that the change in [CO_2] during the mixing process is not conservative, so it cannot be calculated directly by end-member mixing (as DIC can be calculated), and it is necessary to calculate the DIC_{mix}, $DIC_{mix\text{-}ocean}$, TA_{mix}, and $TA_{mix\text{-}ocean}$ and then calculate the corresponding [CO_2] by CO2SYS. In addition, since [CO_2] varies with the water temperature, the temperature was normalized to a mean annual temperature of 24.9℃. The calculation process is shown schematically in Fig. 6b.

Data from Stations J4, J8, J10, J12, and J14 were selected to analyze the composition of [CO_2] and the differences between tides and seasons (Fig. 9). The results show that dissolved CO_2 in the estuary comes primarily from riverine [CO_2], especially at Station J4 in the upper and J8 in the middle which were close to the riverine source. At these locales, [CO_2] were observed to be nearly exclusively supplied by the river (Fig. 9). In contrast, at Stations J12 and J14, where the sea surface became more expansive downestuary, the riverine contribution diminished while estuarine [CO_2] produced by biogeochemical processes became a notable component. Thus, the interplay of external and internal carbon dioxide sources shifted longitudinally in tandem with the fluctuating hydrodynamic dominance of marine versus riverine discharges under changing tidal and geomorphological influences.

Riverine [CO_2] was highest in summer, second highest in autumn, and lowest in winter, and its variation aligned with fluctuation in river discharge (Fig. 3). However, riverine inputs were severely attenuated at high tide, which greatly curtails riverine action, and the magnitude of tidal action surpassed seasonal variation. Within a one-day's tidal cycle, the contribution of riverine [CO_2] to total [CO_2] was twice as pronounced during low tide compared to high tide, whereas the seasonal difference amounted to merely half of that. These findings underscore the overriding dominance of tidally modulated hydrodynamics relative to seasonal shifts in governing estuarine carbon dioxide distribution.

Furthermore, the sample [CO_2] was lower than the conservative mixing [CO_2] between the river and the ocean in autumn and winter in areas of lower salinity (S < 15, Figs 9 and 10), indicated that [CO_2] produced within estuaries through biogeochemical processes such as aerobic respiration could not compensate for the depletion caused by the release of CO_2 to the atmosphere. In

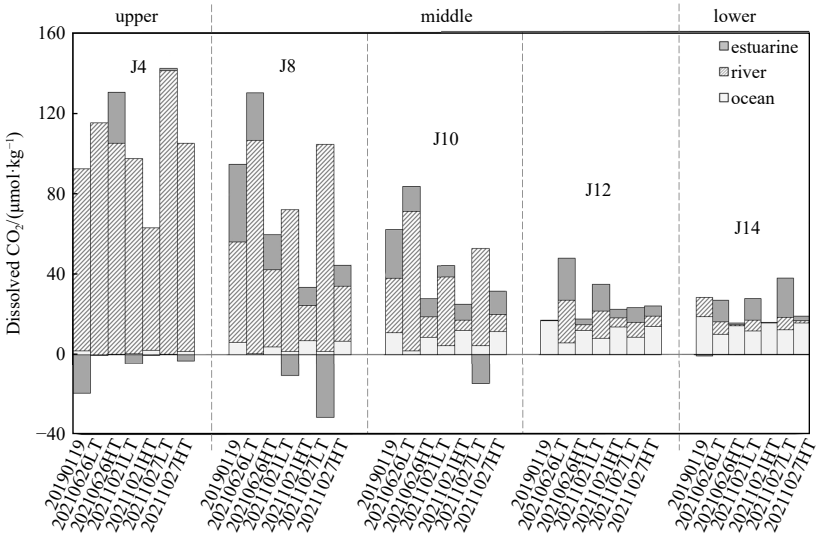

Fig. 9. Histogram of the proportion of [CO_2] composition in the estuary. HT: high tide; LT: low tide.

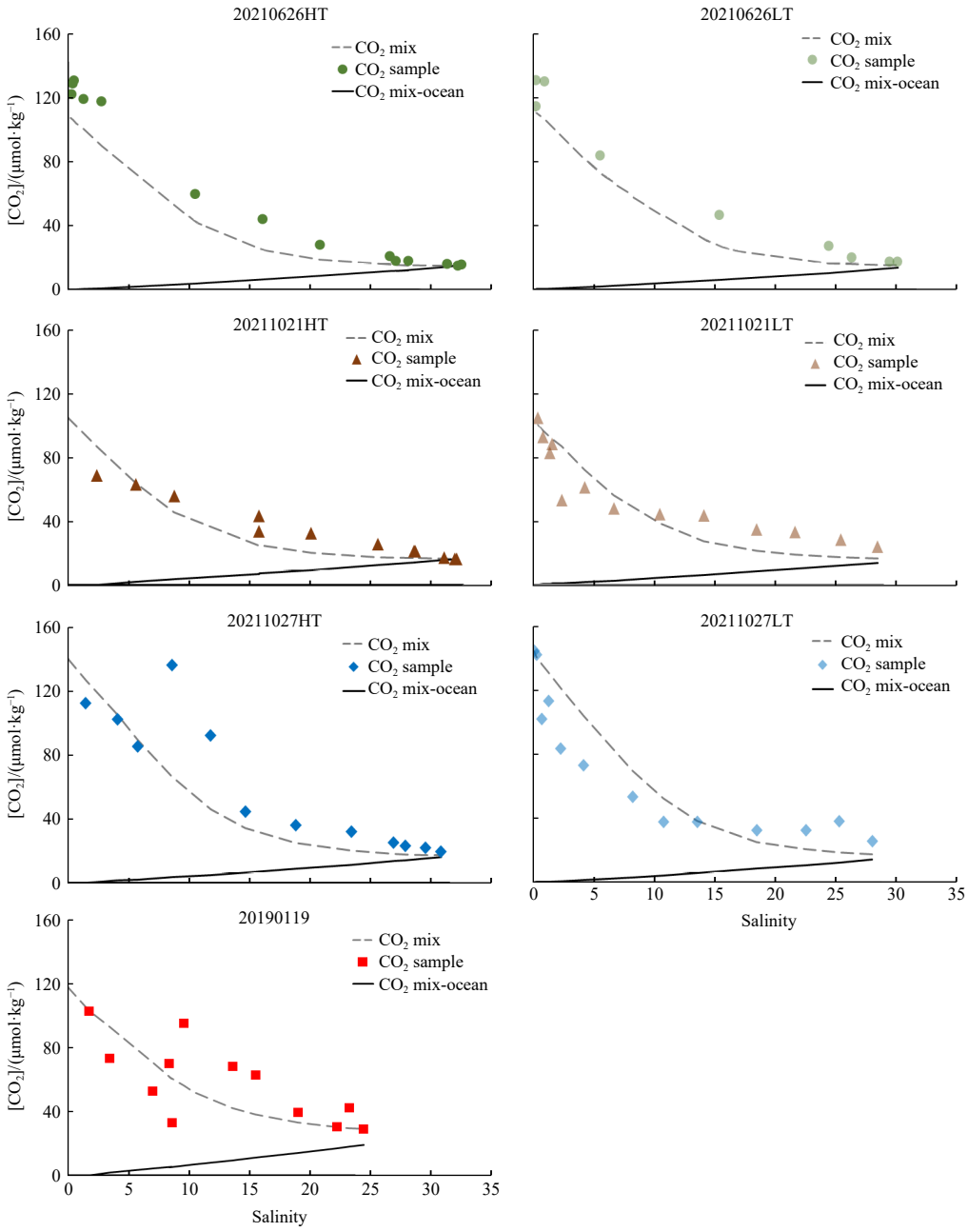

Fig. 10. Variations of $[CO_2]$ with salinity, the grey dashed line represents the $[CO_2]$ from the conservative mixing of the river with the ocean, and the black solid line represents the $[CO_2]$ provided by the ocean in the mixing. HT: high tide; LT: low tide.

addition, the calculated results show that $[CO_2]$ generated in the estuary is also an important source of $[CO_2]$ in the JRE, and the contribution of estuarine $[CO_2]$ is enhanced during high tides.

4.3 *Factors affecting air-sea CO_2 fluxes in the JRE*

Air-sea CO_2 fluxes in estuarine ecosystems are usually influenced by a combination of factors, such as wind, turbulence, tidal currents, and water depth. Ho et al. (2011) used the $^3He/SF_6$ dual tracer technique in the strongly tidal Hudson River Estuary and demonstrated that wind was the main driver of gas exchange in the tidal Hudson River; other factors were negligible. In the JRE, where as another shallow estuary strongly influenced by tides, wind may also be the significant factor constraining air-sea CO_2 flux. However, the Ho model overemphasizes the role of wind speed, and if the wind speed is too low on the day of sampling, the calculated flux will be underestimated. While tidal oscillations exert primacy in propelling fluid motions through estuarine systems, additional hydrodynamic forces modulate gas transfer dynamics at the air-water interface. Current velocity was also an influencing factor should be considered in tidal estuary (Ho et al., 2016). Especially under low to moderate wind conditions, current velocity may even be a driver of gas exchange in shallow tidal estuary (Rosentreter et al., 2017). In this study, three parametric equations with different wind speeds proposed for shallow estuaries (Van Dam et al., 2019; Ho et al., 2011; Jiang et al., 2008), were used to estimate the transport rate of CO_2, and an averaging process was applied to these three models for the estimation of air-sea CO_2 fluxes. In this study, wind speeds on the sampling days were not high, which resulted in low fluxes calculated by the Ho2011 model; therefore, the air-sea CO_2 fluxes calculated

in this study may be smaller than they actually are in the JRE.

CO_2 exchange fluxes were higher in summer and autumn than in winter, partly because of lower wind speeds (1.6 m/s) on the day of sampling in winter and partly because of lower CO_2 exchange rates. Temperature is an important limiting factor for gas exchange rates (Raymond and Cole, 2001), and lower surface water temperatures in winter result in lower air-sea CO_2 exchange rates, leading to lower CO_2 emissions. In contrast, a significant increase in surface water temperature in summer and autumn, combined with relatively high wind speeds on the sampling days, led to a further increase in CO_2 emissions.

By averaging the fluxes in different seasons, the annual mean air-sea CO_2 fluxes in the JRE were estimated to be approximately (25.63 ± 10.25) mol/(m^2·a). Compared with estuaries in other regions of the world (Table 5), the results show that estimated annual mean air-sea CO_2 exchange fluxes in the JRE are slightly lower than those in the Modaomen Estuary in the Zhujiang River basin and higher than those in the Changjiang River and Huanghe River estuaries. Compared with other low-latitude estuaries in the world, CO_2 fluxes in the JRE remain at an intermediate level. The air-sea CO_2 fluxes in the JRE are similar to the average release by tidally influenced estuaries at low and middle latitudes, as suggested by Laruelle et al. (2013) and lower than the spatially limited estuarine fluxes suggested by Chen et al. (2012).

Table 5. The sea surface pCO_2 and air-sea CO_2 fluxes from different estuaries in the world

Estuary	Country	Area/km^2	pCO_2/μatm	CO_2 flux/(mol·m^{-2}·a^{-1})	Reference
Jiulong River Estuary	China	110	530–7 715	25.7	This study
Modaomen Estuary	China	1 012	–	30.8	Tang et al. (2018)
Changjiang River Estuary	China	10 800	650–4 600	14.6	Zhai et al. (2007)
Huanghe River Estuary	China	1 521	–	6.14	Shen et al. (2020)
Hooghly estuary	India	325	559–3 679	47.3	Akhand et al. (2022)
Mekong inner estuary	Vietnam	–	–	44.2	Borges et al. (2018)
Tagus estuary	Portugal	320	487–4 575	33.6	Oliveira et al. (2017)
Elbe inner estuary	Germany	276	380–2 200	40.4	Amann et al. (2015)
Guadalquivir estuary	Spain	39	520–3 606	31.1	De la Paz et al. (2007)
Coffs Creek estuary	Australia	–	403–7 920	18.4	Jeffrey et al. (2018)
Neuse River Estuary	US	455	196–2 510	4.7	Crosswell et al. (2012)

Note: – represents data have not been mentioned in the reference.

5 Conclusions

In this study, we investigated the carbonate system and its controlling factors in the subtropical JRE during the tidal cycle. Additionally, we assessed the magnitude of air-sea CO_2 fluxes within the JRE for the first time, expanding our understanding of carbon cycling within small subtropical estuaries. The carbonate system in the JRE exhibited high spatial and temporal variability. DIC and TA steadily increased, whereas the pCO_2 progressively declined from summer to winter as a result of seasonal variation in runoff. DIC and TA rose continuously, while the pCO_2 dramatically dropped from the upper to the lower estuary. We also quantified the composition of estuarine DIC and dissolved CO_2. The results indicate that the conservative mixing of river water and seawater is the dominant factor that controls carbonate systems during estuarine mixing. Minor controlling factors include aerobic respiration, release of CO_2 from the estuary, groundwater input, and precipitation or dissolution of calcium carbonate.

Within a one-day tidal cycle, there was significant variability in the CO_2 system. Variation in carbonate parameters between low tide and high tide occurred at identical stations. The magnitude of these differences ranged from approximately 15% to 30% for DIC and TA, while for the pCO_2, the divergence reached approximately 30% to 40%. The differences caused by tidal variation were most pronounced in the middle estuary, where the magnitude of changes in DIC and TA at Station J8 approached 40% and alterations in the pCO_2 were even more profound, nearing approximately 60%. These tidal-induced discrepancies surpass the effects of other concurrent processes, thereby emphasizing the importance of investigating tidal variation in estuaries subject to strong tidal influences. Neglecting to do so may lead to egregious overestimations or underestimations of the genuine state of an estuarine system.

References

Abril G, Borges A V. 2005. Carbon dioxide and methane emissions from estuaries. In: Tremblay A, Varfalvy L, Roehm C, et al., eds. Greenhouse Gas Emissions—Fluxes and Processes: Hydroelectric Reservoirs and Natural Environments. Berlin, Heidelberg: Springer, 187–207

Akhand A, Chanda A, Watanabe K, et al. 2022. Drivers of inorganic carbon dynamics and air–water CO_2 fluxes in two large tropical estuaries: Insights from coupled radon (^{222}Rn) and pCO_2 surveys. Limnology and Oceanography, 67(S2): S118–S132

Amann T, Weiss A, Hartmann J. 2015. Inorganic carbon fluxes in the Inner Elbe Estuary, Germany. Estuaries and Coasts, 38(1): 192–210, doi: 10.1007/s12237-014-9785-6

Borges A V, Abril G, Bouillon S. 2018. Carbon dynamics and CO_2 and CH_4 outgassing in the Mekong delta. Biogeosciences, 15(4): 1093–1114, doi: 10.5194/bg-15-1093-2018

Borges A V, Delille B, Frankignoulle M. 2005. Budgeting sinks and sources of CO_2 in the coastal ocean: Diversity of ecosystems counts. Geophysical Research Letters, 32(14): L14601

Cai Weijun, Dai Minhan, Wang Yongchen. 2006. Air-sea exchange of carbon dioxide in ocean margins: A province-based synthesis. Geophysical Research Letters, 33(12): L12603

Chen Chen-Tung Arthur, Huang Ting-Hsuan, Chen Y C, et al. 2013. Air–sea exchanges of CO_2 in the world's coastal seas. Biogeosciences, 10(10): 6509–6544, doi: 10.5194/bg-10-6509-2013

Chen Chen-Tung Arthur, Huang Ting-Hsuan, Fu Yu-Han, et al. 2012. Strong sources of CO_2 in upper estuaries become sinks of CO_2 in large river plumes. Current Opinion in Environmental Sustainability, 4(2): 179–185, doi: 10.1016/j.cosust.2012.02.003

Crosswell J R, Wetz M S, Hales B, et al. 2012. Air-water CO_2 fluxes in the microtidal Neuse River estuary, North Carolina. Journal of Geophysical Research: Oceans, 117(C8): C08017

Dai Minhan, Lu Zhongming, Zhai Weidong, et al. 2009. Diurnal variations of surface seawater pCO_2 in contrasting coastal environments. Limnology and Oceanography, 54(3): 735–745, doi: 10.4319/lo.2009.54.3.0735

De la Paz M, Gómez-Parra A, Forja J. 2007. Inorganic carbon dynamic and air-water CO_2 exchange in the Guadalquivir Estuary (SW

Iberian Peninsula). Journal of Marine Systems, 68(1–2): 265–277, doi: 10.1016/j.jmarsys.2006.11.011

Gattuso J P, Frankignoulle M, Wollast R. 1998. Carbon and carbonate metabolism in coastal aquatic ecosystems. Annual Review of Ecology and Systematics, 29: 405–434, doi: 10.1146/annurev.ecolsys.29.1.405

Gran G, Dahlenborg H, Laurell S, et al. 1950. Determination of the equivalent point in potentiometric titrations. Acta Chemica Scandinavica, 4: 559–577, doi: 10.3891/acta.chem.scand.04-0559

Guo Xianghui, Cai Weijun, Zhai Weidong, et al. 2008. Seasonal variations in the inorganic carbon system in the Pearl River (Zhujiang) estuary. Continental Shelf Research, 28(12): 1424–1434, doi: 10.1016/j.csr.2007.07.011

Hellings L, Dehairs F, Van Damme S, et al. 2001. Dissolved inorganic carbon in a highly polluted estuary (the Scheldt). Limnology and Oceanography, 46(6): 1406–1414, doi: 10.4319/lo.2001.46.6.1406

Ho D T, Coffineau N, Hickman B, et al. 2016. Influence of current velocity and wind speed on air-water gas exchange in a mangrove estuary. Geophysical Research Letters, 43(8): 3813–3821, doi: 10.1002/2016GL068727

Ho D T, Schlosser P, Orton P M. 2011. On factors controlling air-water gas exchange in a large tidal river. Estuaries and Coasts, 34(6): 1103–1116, doi: 10.1007/s12237-011-9396-4

Jahnke R A, Alexander C R, Kostka J E. 2003. Advective pore water input of nutrients to the Satilla River Estuary, Georgia, USA. Estuarine, Coastal and Shelf Science, 56(3–4): 641–653

Jeffrey L C, Maher D T, Santos I R, et al. 2018. The spatial and temporal drivers of pCO_2, pCH_4 and gas transfer velocity within a subtropical estuary. Estuarine, Coastal and Shelf Science, 208: 83–95

Jiang Liqing, Cai Weijun, Wang Yongchen. 2008. A comparative study of carbon dioxide degassing in river- and marine-dominated estuaries. Limnology and Oceanography, 53(6): 2603–2615, doi: 10.4319/lo.2008.53.6.2603

Laruelle G G, Dürr H H, Lauerwald R, et al. 2013. Global multi-scale segmentation of continental and coastal waters from the watersheds to the continental margins. Hydrology and Earth System Sciences, 17(5): 2029–2051, doi: 10.5194/hess-17-2029-2013

Lewis E R, Wallace D W R. 1998. Program developed for CO_2 system calculations. ORNL/CDIAC-105, Carbon Dioxide Information Analysis Center, Oak Ridge National Laboratory, US Department of Energy, Oak Ridge, Tennessee

Li Gong, Gao Kunshan, Yuan Dongxing, et al. 2011. Relationship of photosynthetic carbon fixation with environmental changes in the Jiulong River estuary of the South China Sea, with special reference to the effects of solar UV radiation. Marine Pollution Bulletin, 62(8): 1852–1858, doi: 10.1016/j.marpolbul.2011.02.050

Li Yuhong, Luo Yang, Liu Jian, et al. 2023. Sources and sinks of N_2O in the subtropical Jiulong River Estuary, Southeast China. Frontiers in Marine Science, 10: 1138258, doi: 10.3389/fmars.2023.1138258

Li Chenglong, Zhai Weidong, Qi Di. 2022. Unveiling controls of the latitudinal gradient of surface pCO_2 in the Kuroshio Extension and its recirculation regions (northwestern North Pacific) in late spring. Acta Oceanologica Sinica, 41(5): 110–123, doi: 10.1007/s13131-021-1949-1

Li Yuhong, Zhan Liyang, Chen Liqi, et al. 2021. Spatial and temporal patterns of methane and its influencing factors in the Jiulong River estuary, southeastern China. Marine Chemistry, 228: 103909, doi: 10.1016/j.marchem.2020.103909

Lin Hui. 2012. Seasonal and spatial variation of dissolved inorganic and organic carbon in Taiwan Strait and the Adjacent Sea Area (in Chinese)[dissertation]. Xiamen: Xiamen University

Liu Qian, Dong Xu, Chen Jinshun, et al. 2019. Diurnal to interannual variability of sea surface pCO_2 and its controls in a turbid tidal-driven nearshore system in the vicinity of the East China Sea based on buoy observations. Marine Chemistry, 216: 103690, doi: 10.1016/j.marchem.2019.103690

Millero F J. 2010. Carbonate constants for estuarine waters. Marine and Freshwater Research, 61(2): 139–142, doi: 10.1071/MF09254

Oliveira A P, Cabeçadas G, Mateus M D. 2017. Inorganic carbon distribution and CO_2 fluxes in a large European estuary (Tagus, Portugal). Scientific Reports, 7(1): 7376, doi: 10.1038/s41598-017-06758-z

Orr J, Epitalon J M, Gattuso J P. 2015. Comparison of ten packages that compute ocean carbonate chemistry. Biogeosciences, 12(5): 1483–1510, doi: 10.5194/bg-12-1483-2015

Pritchard D W. 1967. What is an estuary: physical viewpoint. In: Lauff G H, ed. Estuaries. Washington: American Association for the Advancement of Science

Raymond P A, Cole J J. 2001. Gas exchange in rivers and estuaries: Choosing a gas transfer velocity. Estuaries, 24(2): 312–317, doi: 10.2307/1352954

Ries J B. 2011. A physicochemical framework for interpreting the biological calcification response to CO_2 induced ocean acidification. Geochimica et Cosmochimica Acta, 75(14): 4053–4064, doi: 10.1016/j.gca.2011.04.025

Rosentreter J A, Maher D T, Ho D T, et al. 2017. Spatial and temporal variability of CO_2 and CH_4 gas transfer velocities and quantification of the CH_4 microbubble flux in mangrove dominated estuaries. Limnology and Oceanography, 62(2): 561–578, doi: 10.1002/lno.10444

Samanta S, Dalai T K, Pattanaik J K, et al. 2015. Dissolved inorganic carbon (DIC) and its $\delta^{13}C$ in the Ganga (Hooghly) River estuary, India: Evidence of DIC generation via organic carbon degradation and carbonate dissolution. Geochimica et Cosmochimica Acta, 165: 226–248, doi: 10.1016/j.gca.2015.05.040

Shen Xiaomei, Su Meirong, Sun Tao, et al. 2020. Net heterotrophy and low carbon dioxide emissions from biological processes in the Yellow River Estuary, China. Water Research, 171: 115457, doi: 10.1016/j.watres.2019.115457

Sun Heng, Gao Zhongyong, Qi Di, et al. 2020. Surface seawater partial pressure of CO_2 variability and air-sea CO_2 fluxes in the Bering Sea in July 2010. Continental Shelf Research, 193: 104031, doi: 10.1016/j.csr.2019.104031

Sun Heng, Gao Zhongyong, Zhao Derong, et al. 2021. Spatial variability of summertime aragonite saturation states and its influencing factor in the Bering Sea. Advances in Climate Change Research, 12(4): 508–516, doi: 10.1016/j.accre.2021.04.001

Takahashi T, Olafsson J, Goddard J G, et al. 1993. Seasonal variation of CO_2 and nutrients in the high-latitude surface oceans: A comparative study. Global Biogeochemical Cycles, 7(4): 843–878, doi: 10.1029/93GB02263

Takahashi T, Sutherland S C, Sweeney C, et al. 2002. Global sea-air CO_2 flux based on climatological surface ocean pCO_2, and seasonal biological and temperature effects. Deep-Sea Research Part II: Topical Studies in Oceanography, 49(9–10): 1601–1622, doi: 10.1016/S0967-0645(02)00003-6

Takahashi T, Sutherland S C, Wanninkhof R, et al. 2009. Climatological mean and decadal change in surface ocean pCO_2, and net sea-air CO_2 flux over the global oceans. Deep-Sea Research Part II: Topical Studies in Oceanography, 56(8–10): 554–577, doi: 10.1016/j.dsr2.2008.12.009

Tang Wenkui, Gao Quanzhou, Zheng Xiongbo, et al. 2018. Air-water CO_2 exchange fluxes and its controlling mechanism in Modaomen Estuary of the Pearl River, China. Ekoloji, 27(106): e601

Van Dam B R, Edson J B, Tobias C. 2019. Parameterizing air-water gas exchange in the shallow, microtidal New River estuary. Journal of Geophysical Research: Biogeosciences, 124(7): 2351–2363, doi: 10.1029/2018JG004908

Walsh J J. 1988. On the Nature of Continental Shelves. New York: Academic Press, 367–437

Wang Guizhi, Wang Zhangyong, Zhai Weidong, et al. 2015. Net subterranean estuarine export fluxes of dissolved inorganic C, N, P, Si, and total alkalinity into the Jiulong River estuary, China. Geochimica et Cosmochimica Acta, 149: 103–114, doi: 10.1016/j.gca.2014.11.001

Wang Zhaohui, Wanninkhof R, Cai Weijun, et al. 2013. The marine

inorganic carbon system along the Gulf of Mexico and Atlantic coasts of the United States: Insights from a transregional coastal carbon study. Limnology and Oceanography, 58(1): 325–342, doi: 10.4319/lo.2013.58.1.0325

Weiss R F. 1974. Carbon dioxide in water and seawater: the solubility of a non-ideal gas. Marine Chemistry, 2(3): 203–215, doi: 10.1016/0304-4203(74)90015-2

Wu Gaojie, Cao Wenzhi, Huang Zheng, et al. 2017. Decadal changes in nutrient fluxes and environmental effects in the Jiulong River Estuary. Marine Pollution Bulletin, 124(2): 871–877, doi: 10.1016/j.marpolbul.2017.01.071

Yan Xiuli, Zhai Weidong, Hong Huasheng, et al. 2012. Distribution, fluxes and decadal changes of nutrients in the Jiulong River Estuary, Southwest Taiwan Strait. Chinese Science Bulletin, 57(18): 2307–2318, doi: 10.1007/s11434-012-5084-4

Yin Xijie, Lin Yunpeng, Liang Cuicui, et al. 2020. Source and fate of dissolved inorganic carbon in Jiulong River, southeastern China. Estuarine, Coastal and Shelf Science, 246: 107031

Zhai Weidong, Dai Minhan, Guo Xianghui. 2007. Carbonate system and CO_2 degassing fluxes in the inner estuary of Changjiang (Yangtze) River, China. Marine Chemistry, 107(3): 342–356, doi: 10.1016/j.marchem.2007.02.011

Zheng Senlin, Qiu Xiaoyan, Chen Bin, et al. 2011. Antibiotics pollution in Jiulong River estuary: Source, distribution and bacterial resistance. Chemosphere, 84(11): 1677–1685, doi: 10.1016/j.chemosphere.2011.04.076